
Proceedings Paper:
Woolley, RM, Fairweather, M, Wareing, CJ et al. (2014) Application of Turbulence Closures and Thermodynamic Approaches in the RANS Modelling of High-Pressure CO2 Releases. In: Proceedings of the 10th International ERCOFTAC Symposium on Engineering Turbulence Modelling and Measurements – ETMM10. 10th International ERCOFTAC Symposium on Engineering Turbulence Modelling and Measurements – ETMM10, 17-19 Sep 2014, Don Carlos Resort, Marbella, Spain.

Application of Turbulence Closures and Thermodynamic Approaches in the RANS Modelling of High-pressure CO_2 Releases

R.M. Woolley[1], M. Fairweather[1], C.J. Wareing[1, 2], S.A.E.G. Falle[2], I. Economou[3], D. Tsangaris[3], G. Boulougouris[3], C. Proust[4], D. Jamois[4], J. Hebrard[4]

[1]School of Process, Environmental and Materials Engineering, University of Leeds, Leeds LS2 9JT, UK
[2]School of Mathematics, University of Leeds, Leeds LS2 9JT, UK
[3]National Center for Scientific Research "Demokritos", Institute of Physical Chemistry, Molecular Thermodynamics and Modelling of Materials Laboratory, GR–153 10 Aghia Paraskevi, Attikis, Greece
[4]INERIS, Dept. PHDS, Parc Technologique ALATA, BP 2, 60550 Verneuil-en-Halatte, France

r.m.woolley@leeds.ac.uk

1 Introduction

Pipelines are considered to be the most likely method for transportation of captured CO_2 from power plants and other industries prior to subsequent storage, and their safe operation is of paramount importance as the contents would likely be several thousand tonnes. CO_2 poses a number of dangers upon release due to its physical properties. It is a colourless and odourless asphyxiant which has a tendency to sublimation and solid formation, and is directly toxic in inhaled air.

Following the puncture or rupture of a CO_2 pipeline, a gas-liquid droplet mixture or gas alone will be released to atmosphere and disperse over large distances. This may be then followed by gas-solid discharge during the latter stages of pipeline depressurisation due to the significant degree of cooling taking place. The possibility of releases of three-phase mixtures also exists. This paper focuses on the detailed mathematical modelling of the near-field characteristics of these complex releases, since predictions of major hazards used in risk assessments are based on the use of near-field source terms that provide input to far-field dispersion models.

Because the pre- to post-expansion pressure ratio resulting from a release will initially be large, the sonic velocity will be reached at the outlet of the pipeline and the resulting free jet will be sonic. This pressure difference leads to a complex shock cell structure within the jet which for the initial highly under-expanded flow will give rise to a flow that contains a Mach disk followed by a series of shock diamonds as it gradually adjusts to ambient conditions.

The results presented in this paper provide new insight into the complex interactions of turbulence and phase-behaviour observed in such releases.

2 Experimental measurement

Figure 1 is a schematic of the rig used at INERIS for the experimental studies of large-scale CO_2 releases, with the external release point on the right of the picture. This is connected to the main vessel via a discharge line of 50 mm inner diameter, with no internal restrictions. In total, the line is 9 metres long including a bend inside the vessel, plunging to the bottom in order to ensure that it is fully submersed in liquid CO_2.

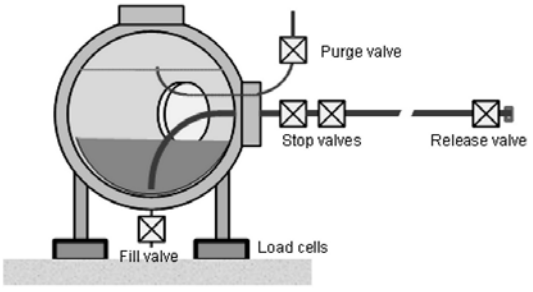

Figure 1: Schematic of INERIS experimental rig used to investigate large-scale CO_2 releases.

The 2 cubic metre spherical pressure vessel is thermally insulated, and can contain up to 1000

kg of CO_2 at a maximum operating pressure and temperature of 200 bar and 473 K, respectively. It is equipped internally with 6 thermocouples and 2 high-precision pressure gauges. The vessel has a mass of approximately 5000 kg, and is supported by 4 'Mettler 0745 A' load cells, enabling a continuous measurement of the CO_2 content with an uncertainty of ±500 g.

The field instrumentation in the dispersion zone consists of eighteen radially- distributed 0.5 mm diameter K-type thermocouples arranged on vertical masts at varying distances from the orifice, which have response times of approximately one second. In addition to this, three oxygen sensors are distributed along the centre-line axis of the jet. Furthermore, apparatus was constructed to capture some of the very near-field behaviour of the jet, and results obtained from this are presented later in the paper alongside model predictions. This apparatus supported thermocouples lying along the jet centre-line at locations of 0.06, 0.16, 0.26, and 0.36 m beyond the release plane.

3 Turbulent flow modelling

Predictions were based upon the solution of the ensemble-averaged, density-weighted forms of the transport equations for mass, momentum, and total energy. Solutions were obtained of the axisymmetric forms of these descriptive equations, and their integration employed a second-order accurate, upwind, finite-volume scheme in which they were discretised following a conservative control-volume approach with values of the dependent variables being stored at the computational cell centres. Approximation of the diffusion and source terms was undertaken using central differencing, and an HLL (Harten, Lax, van Leer) (Harten et al., 1983) second-order accurate variant of Godunov's method applied with respect to the convective and pressure fluxes. The calculations also employed an adaptive finite-volume grid algorithm which uses a two- or three-dimensional rectangular mesh with grid adaption achieved by the successive overlaying of refined layers of computational mesh. A further explanation of the solution algorithm can be found in Falle (1991).

Discussed above are the standard equations used for modelling fluid flow, and these require a turbulence model to effect closure of the system. In this paper, a two-equation model and a second-moment transport model are used to represent the turbulence components. Models are used to represent the Reynolds stresses, and in the first instance, this is undertaken using the k-ε approach (Jones and Launder, 1972). Although the standard k-ε model has been extensively used for the prediction of incompressible flows, its performance is well known to be poor in the prediction of their compressible counterparts. The model consistently over-predicts turbulence levels, and hence mixing, in compressible flows displaying an enhancement of turbulence dissipation. A number of modifications to the k-ε model have been proposed by various authors, which include modifications to the constants in the turbulence energy dissipation rate equation, and to the dissipation rate itself. Previous works by the authors (Fairweather and Ranson, 2006) have indicated that for flows typical of those being studied here, the model proposed by Sarkar et al. (1991) provides the most reliable predictions. Additionally,

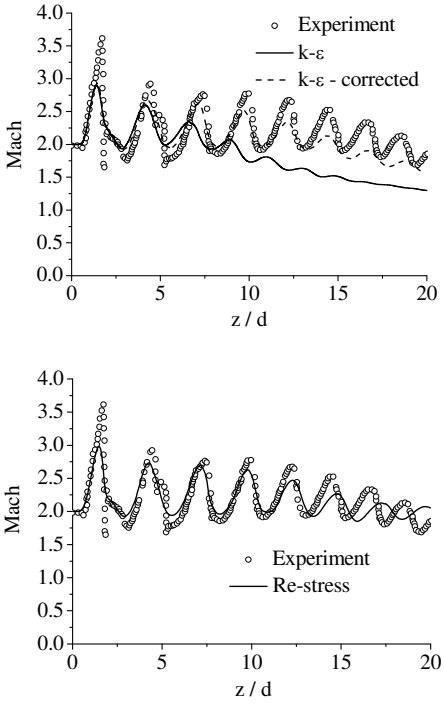

Figure 2: Mach number predictions (top – k-ε, bottom – Reynolds stress) plotted against experimental data.

a Reynolds stress transport model was implemented to represent the effects of turbulence upon the flow field. A number of variations has been analysed in this paper, focussing upon their performance in accounting for the effects of compressibility.

Validation of the turbulence models has been undertaken using data available in the literature, and Figure 2 compares predictions obtained using both the un-modified and the modified k-ε, and the Reynolds stress (Jones and Musonge, 1988) turbulence models against experimental data of the local Mach number, of the moderately under-expanded air jet as reported by Seiner and Norum (1979).

Both two-equation models predict the presence of the initial series of oblique shocks in the very

near field of the jet, but the standard model severely over-predicts the dissipation of these shocks with downstream progression due to over-prediction of turbulence levels. The Reynolds stress model is seen to be a considerable improvement over the k-ε model in that the magnitude and frequency of the variation is in better agreement with experimental data without any modification for compressible effects. The effects of an overly-dissipative solution are however seen to appear at approximately 15

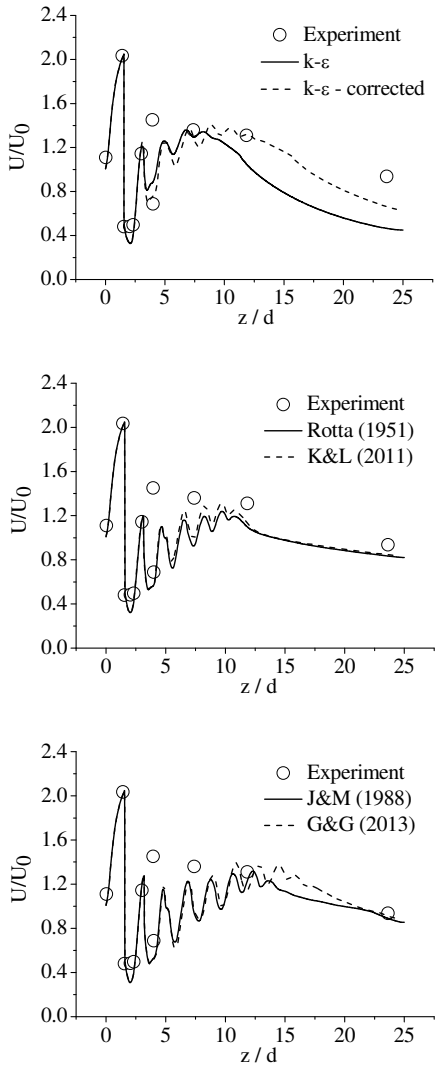

Figure 3: Normalised velocity predictions (top – k-ε, middle and bottom – Reynolds stress) plotted against experiment.

nozzle diameters where the amplitude of the predicted oscillations begins to rapidly decay, and a discrepancy can also be seen with respect to the wave frequency.

It is now widely accepted that the main contributor to the structural compressibility effects is the pressure-strain term (Π_{ij}) appearing in the transported Reynolds stress equations (Sarkar, 1995). Hence, the use of compressible dissipation models is now considered physically inaccurate, although their performance is good.

Ignoring the rapid part of the pressure-strain correlation, Rotta (1951) models the term as Equation (1) where ε is the dissipation of turbulence kinetic energy, and b_{ij} is the Reynolds stress anisotropy, as defined in the first term of Equation (3) below:

$$\Pi_{ij} = -C_1 \varepsilon b_{ij} \tag{1}$$

Later, this model was extended (Khlifi and Lili, 2011) to directly incorporate terms arising from compressibility effects as Equation (2):

$$\Pi_{ij} = -C_1 \left(1 - \beta M_t^2\right) \varepsilon b_{ij} \tag{2}$$

where βM_t is a function of the turbulent Mach number, vanishing in an incompressible flow.

Prior to this development, Jones and Musonge (1988) provide a model to account for the 'rapid' element of the correlation. Defining a function for the fourth-rank linear tensor in the strain-containing term with the necessary symmetry properties, they obtain:

$$\begin{aligned}\Pi_{ij} = &-C_1 \varepsilon \left(\frac{\bar{\rho} \widetilde{u_i'' u_j''}}{k} - \frac{2}{3} \delta_{ij} \bar{\rho} \right) + C_2 \delta_{ij} \bar{\rho} \widetilde{u_i'' u_j''} \frac{\partial \tilde{u}_k}{\partial x_l} \\ &- C_3 P_{ij} + C_4 \bar{\rho} k \left(\frac{\partial \tilde{u}_i}{\partial x_j} + \frac{\partial \tilde{u}_j}{\partial x_i} \right) + C_5 \bar{\rho} \widetilde{u_i'' u_j''} \frac{\partial \tilde{u}_l}{\partial x_l} \\ &+ C_6 \left(\bar{\rho} \widetilde{u_k'' u_j''} \frac{\partial}{\partial x_k} \left(\tilde{u}_k \right) + \bar{\rho} \widetilde{u_k'' u_i''} \frac{\partial}{\partial x_j} \left(\tilde{u}_k \right) \right) \\ &+ C_7 \bar{\rho} k \delta_{ij} \frac{\partial \tilde{u}_l}{\partial x_l}\end{aligned} \tag{3}$$

where the C_1 term corresponds to the 'slow' part as previously defined as Equation (1), k is the turbulence kinetic energy, $\bar{\rho}$ the mean density, δ_{ij} the Kroncker delta, and $\widetilde{u''u''}$ and $\tilde{u}$ the Favre-averaged Reynolds stresses and velocity components, respectively.

Defining the gradient and turbulent Mach numbers as:

$$M_g \equiv \frac{Sl}{a} \qquad and \qquad M_t \equiv \frac{\sqrt{2k}}{a} \tag{4}$$

Gomez and Girimaji (2013) introduce corrections to their derivation of Π_{ij} as Equation (5), which is implemented in terms of a modification to Equation (3) in the current work:

$$\Pi_{ij} = -C_1\left(M_t\right)b_{ij} + \sum_k C_k\left(M_g\right)T_{ij}^k \qquad (5)$$

The turbulent Mach number is the ratio of the magnitude of the velocity fluctuations to the speed of sound, and the dependence of the 'slow' part reflects the degree of influence of dilatational fluctuations. The gradient Mach number characterises the shear to acoustic time scales, and its influence upon the 'rapid' part corresponds to the fluctuating pressure field which arises due to the presence of the mean velocity gradient.

Figure 3 depicts the application of these turbulence closures to the prediction of centreline axial velocity, normalised by the magnitude at the nozzle exit, for the highly under-expanded air jet studied by Donaldson and Snedeker (1971). Results obtained using the k-ε model and its associated correction attributed to Sarkar et al. (1991) can be seen to conform with observations previously made with respect to the moderately under-expanded air jet. In this case, the initial shock structure is poorly defined by the standard model, and the over-predicted dissipation of these phenomena is considerable by ten nozzle diameters from the jet outflow. The Sarkar modification to the turbulence dissipation goes some way to reducing the over-prediction up to approximately 15 diameters, but the resolution of the initial shock-laden region remains poor, and the solution subsequently becomes overly dissipative.

The Reynolds stress transport model with the closure of the pressure-strain correlation attributed to Rotta (1951) notably improves upon the resolution of the shock region and the prediction of the dissipation of turbulence kinetic energy. The introduction of a compressible element to the 'slow' part of the model as discussed by Khlifi and Lili (2011) effects an additional increase in peak magnitude predictions in the near field, although has little effect upon the subsequent downstream turbulence dissipation. The application of a model for the 'rapid' part of the pressure-strain term (Jones and Musonge, 1988), incorporated with the simple model of Rotta for the 'slow' part proves a significant improvement with respect to predictions of both the shock resolution and the turbulence dissipation. This is again improved upon by the introduction of corrections based upon the turbulent and gradient Mach numbers as outlined by Gomez and Girimaji (2013).

4 Thermodynamics modelling

The Peng-Robinson (1976) equation of state is satisfactory for modelling the gas phase, but when compared to that of Span and Wagner (1996), it is not so for the condensed phase, as demonstrated by Wareing et al. (2013). Furthermore, it is not accurate for the gas pressure below the triple point and, in common with any single equation, it does not account for the discontinuity in properties at the triple point. In particular, there is no latent heat of fusion. A number of composite equations of state have therefore been constructed by the authors for the purpose of comparing performance in application to practical problems of engineering interest. In these, the gas phase is computed from the Peng-Robinson equation of state, and the liquid phase and saturation pressure are calculated from tabulated data generated with the Span and Wagner equation of state, or from an advanced model based upon statistical associating fluid theory (SAFT) (Diamantonis et al., 2013). Solid phase properties are obtained from an available source of thermodynamic data for CO_2, the Design Institute for Physical Properties (DIPPR) 801 database (http://www.aiche.org/dippr), or from a recently developed model attributed to Jager and Span (2012).

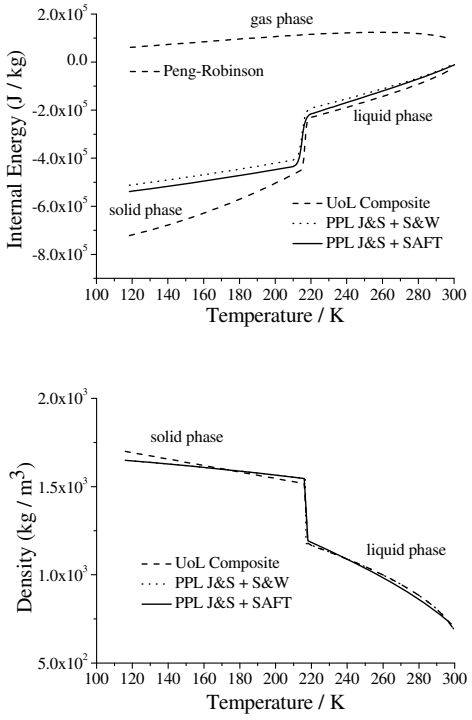

Figure 4: Saturation-line internal energy and density predictions of pure CO_2 using three different equations of state compositions.

Under the remit of the CO2QUEST FP7 project, the development of a Physical Properties Library (PPL), and hence the provision of a 'platform' capable of predicting physical and thermodynamic properties of pure CO_2 and its mixtures, has been undertaken. The PPL contains a collection of models which can be applied regardless of the application, and include a number of

cubic formulations such as those described by Peng and Robinson, and Soave, and the formulation of Span and Wagner. Also available is the analytical equation of Yokozeki (2004), and the advanced molecular models described as SAFT and PC-SAFT by Gross and Sadowski (2001). A comparative study of the performance of these equations of state has been undertaken using experimental data of high-pressure CO_2 releases for validation. Due to space restrictions, a representative sample of these results is presented which include the composite model described above, and the PPL-derived Jager and Span (2012) model coupled with both Span and Wagner (1996) and SAFT. Figure 4 depicts density and internal energy predictions for both the condensed and the gaseous phases on the saturation line for a pure CO_2 system obtained using these three different approaches. Importantly, it can be seen that all models incorporate the latent heat of fusion which must be considered over the liquid-solid phase boundary. They can also be said to similarly represent the internal energy of the liquid phase, although a discrepancy is observed with the composite model. This can be attributed to the inclusion in that model of a small value to ensure conformity with Span and Wagner (1996) in terms of the predicted difference between gas and liquid energies (Wareing et al., 2013). The major discrepancy in predictions lies in the solid-phase region, in that the composite model is in notable disagreement with the models incorporating Jager and Span (2012). This can be attributed to the sources of experimental data used in the derivation of the respective models, and the reader is referred to these papers for further information regarding the data sources.

5 Validation against experimental CO_2 releases

Figure 5 presents sample density and temperature predictions of one of the large-scale test cases used for the validation of the code, obtained using the second-moment turbulence closure (Gomez and Girimaji, 2013) and three of the composite equations of state. Undertaken by INERIS, the experimental parameters were a reservoir pressure of 83 bar, an exit nozzle diameter of 12.0×10^{-3} m, and an observed mass flow rate of 7.7 kg s^{-1}. The predictions are of the very near field of the jet, encompassing the nozzle exit, and in the case of the temperature, extending to 0.5 metres downstream. This equates to a distance of approximately 42 nozzle diameters (d), and the Mach disc can clearly be seen as a step-change in temperature just before 0.1 metres. Temperature predictions are in good quantitative agreement with experimental data within this region, although it is difficult to assess how the model performs qualitatively due to the resolution of the temperature measurements available. The difference in predicted solid-phase properties can be seen to influence the temperature predictions most notably in the region 0.02 metres to 0.1 m, where the composite model predicts a warmer jet. Not unexpectedly, this region coincides with the system passing through the triple point at 216.5 K, being notable by the small step-change in the temperature curve of Figure 5, and the subsequent freezing of the liquid CO_2.

Density predictions derived from the three models appear to be in good agreement within the very near-field, although closer scrutiny of the predictions reveals the effect of the different solid-phase models. Contrary to intuition, the composite equation predicts a slightly higher density in the first 0.03 metres, but conversely predicts a slightly higher temperature in the region bounded by the triple point and the stationary shock. It is considered that this observation is due to two factors. Initially, the predicted density of the liquid release obtained from this model is greater due to the observed differences in the liquid-phase predictions (Figure 4). Subsequently, as the system passes through the triple point, the composite model predicts slightly higher temperatures for the solid-phase, which relates to a small correction in the density, bringing them in to line with the PPL-derived models.

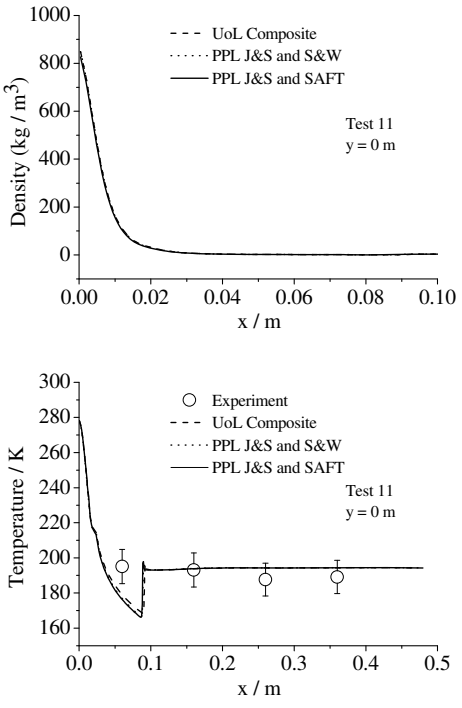

Figure 5: Mean density and temperature predictions of a large scale, sonic release of CO_2 plotted against experimental data.

Further downstream, and with reference to Figure 6, predictions obtained using the Reynolds-stress model of Gomez and Girimaji (2013) and the composite equation of state, are conforming with experimental data both qualitatively and quantitatively, although a slight over-prediction of temperature can be seen across the width of the jet and also with downstream progression. This is indicative of a marginally over-predicted rate of mixing, in-line with previous observations made of the turbulence model validations. It can be said that the second-moment model out-performs the k-ε approach when coupled with the composite equation of state, in that the rate of mixing is better represented. This is manifest as a notable under-prediction of temperatures along the jet axis and also across its width, where the shear layer of the jet is observable as a temperature change of steep gradient, not observed in the Reynolds stress predictions.

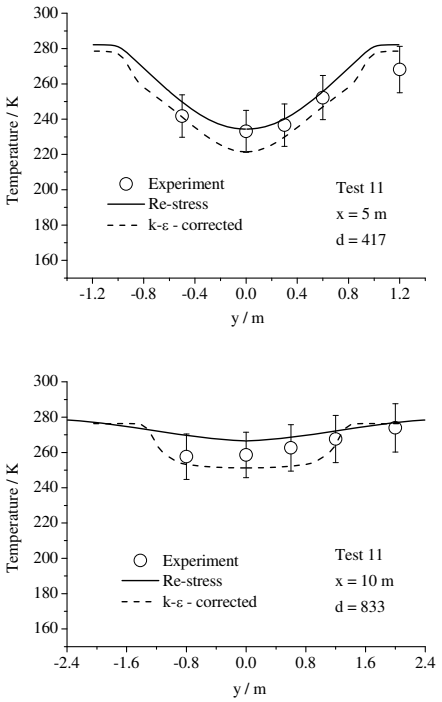

Figure 6: Mean temperature predictions within a large scale, sonic release of CO_2 plotted against experimental data.

6 Conclusions

Presented are sample results from a number of turbulence and thermodynamics models which have been developed to accurately predict the flow structure and phase behaviour of accidental releases of high-pressure CO_2 for engineering applications. An excellent level of agreement between modelling approaches and experimental data has been observed.

Acknowledgements

The research leading to the results contained in this paper received funding from the European Union 7th Framework Programme FP7-ENERGY-2012-1 under grant number 309102. The paper reflects only the authors' views and the European Union is not liable for any use that may be made of the information contained therein.

References

Diamantonis, N.I., Boulougouris, G.C., Mansoor, E., Tsangaris, D.M., Economou, I.G. (2013), Evaluation of Cubic, SAFT, and PC-SAFT Equations of State for the Vapor-liquid Equilibrium Modeling of CO_2 Mixtures with other Gases. *Ind. Eng. Chem. Res.,* Vol. 52, pp. 3933-3942.

Donaldson, C.D., Snedeker, R.S. (1971), A Study of Free Jet Impingement. Part 1. Mean Properties of Free and Impinging Jets. *J. Fluid Mech.,* Vol. 45, pp. 281-319.

Fairweather, M., Ranson, K.R. (2006), Prediction of Underexpanded Jets Using Compressibility-Corrected, Two-Equation Turbulence Models, Prog. Comput. Fluid Dy., Vol. 6, pp. 122-128.

Falle, S.A.E.G. (1991), Self-Similar Jets. *Mon. Not. R. Astron. Soc.,* Vol. 250, pp. 581-596.

Gomez, C.A., Girimaji, S.S. (2013), Toward Second-moment Closure Modelling of Compressible Shear Flows. *J. Fluid Mech.,* Vol. 733, pp. 325-369.

Gross, J., Sadowski, G. (2001), Perturbed-Chain SAFT: An Equation of State Based on a Perturbation Theory for Chain Molecules. *Ind. Eng. Chem. Res.,* Vol. 40, pp. 1244-1260.

Harten, A., Lax, P.D., Leer, B.v. (1983), On Upstream Differencing and Godunov-Type Schemes for Hyperbolic Conservation Laws. *SIAM Rev.,*Vol. 25, pp. 35-61.

Jager, A., Span, R. (2012), Equation of State for Solid Carbon Dioxide Based on the Gibbs Free Energy. *J. Chem. Eng. Data,* Vol. 57, pp. 590-597.

Jones, W.P., Launder, B.E. (1972), The Prediction of Laminarization with a Two-Equation Model of Turbulence. *Int. J. Heat Mass Tran.,* Vol. 15, pp. 301-314.

Jones, W.P., Musonge, P. (1988), Closure of the Reynolds Stress and Scalar Flux Equations. *Phys. Fluids,* Vol. 31, pp. 3589-3604.

Khlifi, H., Lili, T. (2011), A Reynolds Stress Closure for Compressible Turbulent Flow. *JAFM,* Vol. 4, pp. 99-104.

Peng, D.-Y., Robinson, D.B. (1976), A New Two-Constant Equation of State. *Ind. Eng. Chem. Fun.,* Vol. 15, pp. 59-64.

Rotta, J. (1951), Statistische Theorie nichthomogener Turbulenz. 1. Mitteilung. *Z. Phys. A-Hardon Nucl.,* Vol. 129, pp. 547-572.

Sarkar, S. (1995), The Stabilizing Effect of Compressibility in Turbulent Shear Flow. *J. Fluid Mech.,* Vol. 282, pp. 163-186.

Sarkar, S., Erlebacher, G., Hussaini, M.Y., Kreiss, H.O. (1991), The Analysis and Modelling of Dilatational Terms in Compressible Turbulence. *J. Fluid Mech.,* Vol. 227, pp. 473-493.

Seiner, J.M., Norum, T.D. (1979). Experiments of Shock Associated Noise on Supersonic Jets, *AIAA 12th Fluid and Plasma Dynamics Conference*. AIAA, Williamsburg, Virginia.

Span, R., Wagner, W. (1996), A New Equation of State for Carbon Dioxide Covering the Fluid Region from the Triple-Point Temperature to 1100 K at Pressures up to 800 MPa. *J. Phys. Chem. Ref. Data,* Vol. 25, pp. 1509-1596.

Wareing, C.J., Woolley, R.M., Fairweather, M., Falle, S.A.E.G. (2013), A Composite Equation of State for the Modelling of Sonic Carbon Dioxide Jets. *AIChE J.,* Vol. 59, pp. 3928-3942.

Yokozeki, A. (2004), Solid-Liquid-Vapor Phases of Water and Water-Carbon Dioxide Mixtures Using a Simple Analytical Equation of State. *Fluid Phase Equilibr.,* Vol. 222-223, pp. 55-66.